Multiscale Morphological Analysis of Commingled PP/ Unidirectional Glass Fiber Composites: Experiment and Theory

F. Dubouloz-Monnet, P. Mélé, N. D. Albérola

Laboratoire Matériaux Organiques à Propriétés Spécifiques, UMR 5041 CNRS –Université de Savoie, 73376 Le Bourget du Lac Cedex, France

Received 18 March 2004; accepted 27 April 2004
DOI 10.1002/app.21020
Published online in Wiley InterScience (www.interscience.wiley.com).

ABSTRACT: Quantitative 2D image processing has been performed to assess the morphology of commingled polypropylene composites reinforced by a range of glass fiber contents. Quantitative morphological probes, derived from both local and global analyses, point out the heterogeneous dispersion of unidirectional fibers within the polymer matrix, i.e., the presence of aggregates. It is found that more than 86% of fibers are packed into aggregates at a maximum packing fraction of 0.84 whatever the filler content. Moreover, accounting for these morphological characteristics and based on the percolation concept, prediction of the morphology behavior of such composites is proposed. A good agreement between theory and experiment is found. © 2005 Wiley Periodicals, Inc. J Appl Polym Sci 97: 1038–1050, 2005

Key words: composites; morphology; multiscale; simulations; unidirectional

INTRODUCTION

Macroscopic properties of unidirectional composites are usually analyzed through a simplified description of the morphology, i.e., a regular distribution of reinforcing fibers within the polymer matrix.[1] Thus, the fibers are assumed to be periodically disposed according to a square or a hexagonal arrangement. In addition, fibers are considered to be well aligned along the longitudinal axis of the composite.

However, due to particular processing conditions, industrial composite materials, such as epoxy reinforced by unidirectional glass fibers or commingled composites, exhibit heterogeneous morphology characterized by the presence of fiber aggregates.[2–4] The state of aggregation is governed by various factors such as, for example, the respective diameters of fibers,[5,6] the manufacturing conditions,[6–10] or the viscosity of the molten thermoplastic polymers that limit the impregnation of the fillers.[11–15] In addition, some defects of alignment or periodic waves of fibers have been detected as a function of manufacturing conditions.[16–18] To take account of the actual morphology, a new approach has been developed by Albérola et al.[2] to describe the reinforcement mechanisms in these kinds of composite materials.

Correspondence to: P. Mélé (pmele@univ-savoie.fr).

Journal of Applied Polymer Science, Vol. 97, 1038–1050 (2005)

In this paper, by using 2D digital image processing, it is proposed to define accurate analysis probes of the unidirectional fiber geometric arrangement. Subsequently, an actual description and a prediction of the morphology of polypropylene/unidirectional glass fiber composites are proposed at different scales. To this aim, different approaches will be developed through the determination of various morphological parameters such as the distance between the first nearest-neighbor,[19,20] the "included angles" method,[18] or a power spectrum analysis.[21]

EXPERIMENTAL

Materials

A mixture of unmodified PP and maleic anhydride grafted PP under pellet form was extruded and drawn at constant rate to obtain filaments. These were provided by the Vetrotex International Company and the diameter of these polypropylene fibers was found to be 30 ± 2 μm from image analysis (Fig. 1).

According to St. John,[6] when fiber polymer diameters are slightly larger than those of the glass fibers, the processing conditions of commingled composites permit an excellent interdispersion of the two types of fibers.

Unidirectional glass fibers are provided by the Vetrotex International Company and the unimodal distribution of their diameter is centered at about 17.5 ± 0.5 μm. Moreover, Dubouloz-Monnet et al.[3] have shown that the average diameter of glass fibers in

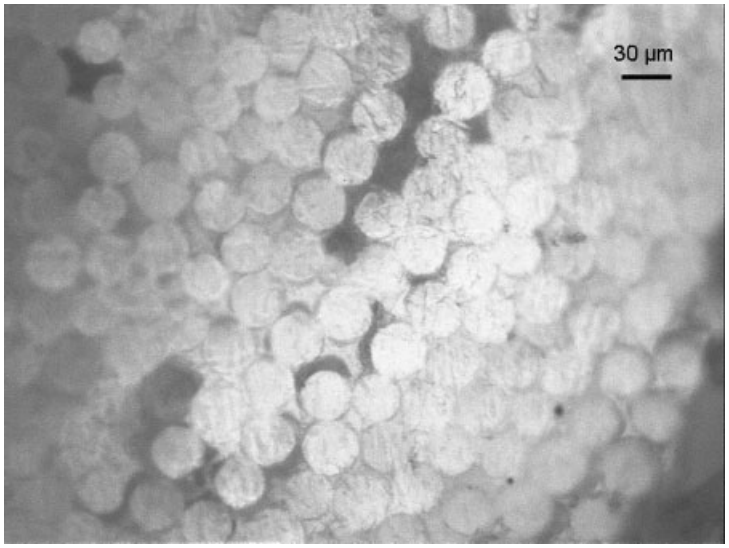

Figure 1 Section of polypropylene filaments.

similar kinds of composites are situated at about the same value, whatever the glass content.

Sample preparation

The Twintex® unidirectional commingled composites are processed starting from bundles gathering several hundred of fibers of polymer and reinforcement.[11,22,23] The sheets of Twintex® composites then are manufactured by filament rolling up. The mixed fibers are then hot consolidated under pressure during an optimal time at a temperature higher than the melting point of polymer. This ensures that the molten polymer can completely impregnate the bundles of glass fibers.[6,7,9,10,23]

Composites showing three glass fiber contents were processed. The weight content of fillers, W_f; the volume fraction, V_f; the corresponding surface of fibers, S_f; and the porosity, S_p, evaluated through different experimental techniques, are presented in Table I, as well as the abbreviations used in the remainder of this paper.

TABLE I
Weight (W_f), Volume (V_f), and Surface (S_f) Fractions of Glass Fibers in the Different Analyzed Composites and Surface Void Content (S_P)

Composite	W_f^a (%)	V_f^b (%)	S_f^c (%)	S_p^d (%)
T22	44.3 ± 0.2	21.6 ± 0.2	21.8 ± 1.7	0.3 ± 0.1
T35	61.5 ± 0.2	35.6 ± 0.2	34.9 ± 2.6	1.6 ± 0.3
T50	74.3 ± 0.1	50.0 ± 0.1	49.9 ± 2.1	1.0 ± 0.2

[a] Determined from residues of burned samples at 625°C.
[b] Derived from weight content.
[c] Determined by image analysis.
[d] Evaluated by image analysis.

Porosity was previously determined through a morphological approach based on image analysis.[24] It is well known that the presence of porosity in composites can lead to a significant decrease in macroscopic properties.[1] To limit the porosity, the Vetrotex International Company has optimized the processing conditions.[6]

We found good agreement between V_f and S_f values, determined, respectively, from residues of burned samples and from image analysis.

The T22 composite exhibits porosity lower than 1%, whereas the T35 composite shows a value close to 2%. In agreement with St. John,[6] the porosity can be regarded as negligible in the rest of this study.

Methods

Optical observations of the samples were carried out in reflexion mode with the help of both a Leitz optical and a Leica TCS SP confocal microscope.

Scanning electron microscopy (SEM) observations were performed on the transversal section of polished and metallized samples by using a Leica Stereoscan 440 scanning electronic microscope. The observations of the samples were carried out in the detection mode of the retrodiffused electrons, to obtain a good contrast between phases.

Quantitative morphological analyses of the composites were undertaken by processing SEM and confocal microscopy observations using various image software, such as ImageJ[25] and Scion Image.[26]

The parameters were determined by using the two following steps:

1. First an adapted threshold permits the removal of the different gray levels in the images ob-

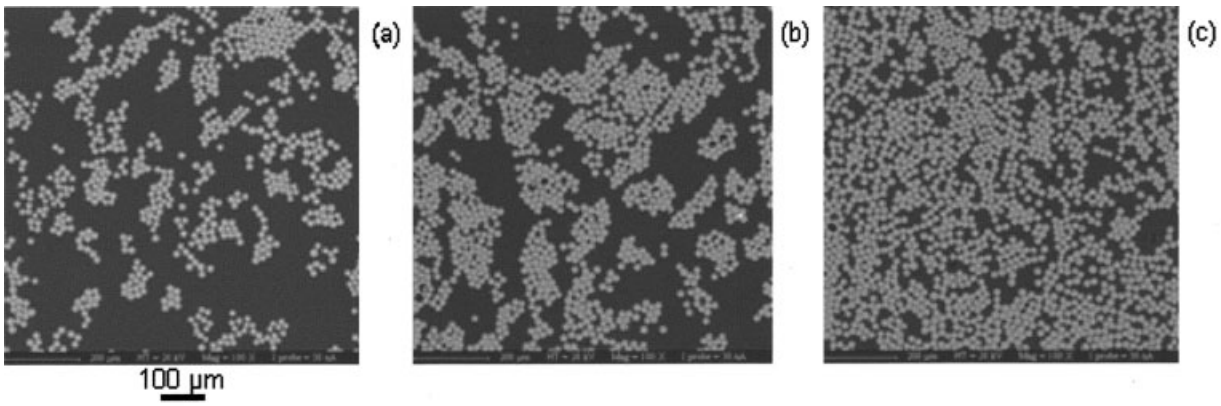

Figure 2 SEM observations of 2D geometric arrangement of fibers in composites (a) T22, (b) T35, and (c) T50.

tained from the various techniques of observation to have binary images, then a mathematical analysis based on iterative algorithms for binary images by operations such as "dilatation," "erosion," "closing," or "opening" was performed. The aims were to evaluate the various phase contents, i.e., glass fibers and aggregates, and the different characteristic distances between these phases.

2. The various parameters reported were taken from a statistical analysis of at least 10 images per filler content including 1,000 glass fibers minimum per image.

RESULTS

Experimental qualitative morphology analysis: 2D spatial distribution of the glass fibers

Figure 2 shows the 2D geometric arrangement of glass fibers within a PP matrix for the different composites. Whatever the surface fraction of filler is, it can be observed that fibers are packed into aggregates. In addition, at this analysis scale, it seems that the interfibre distance in the aggregates remains constant whatever the fiber content. This can also be observed in PBT/glass fiber composites.[4] In contrast for epoxy/unidirectional glass fiber composites, Albérola et al.[2] have shown that the interfiber distance increases as the filler content increases.

Experimental quantitative morphology analysis

At the local scale

Alignment of glass fibers to the longitudinal axis of composites. A previous approach based on the sphericity of fibers evaluated from SEM observations has shown that glass fibers in the materials analyzed are found to be well aligned.[3]

Based on the observations performed by confocal microscopy, a new method has been carried out to confirm this good alignment. For this, the investigated surface, close to 5,600 μm^2 in the (X,Y) plane for focal planes, is analyzed along the (Z) axis from 0 μm, corresponding to the surface of the sample, to a depth of 100 μm (Fig. 3).

The alignment of glass fibers is defined through the subtraction of images located (i) at the top of the specimen and (ii) at 100 μm depth. For example, Figure 3(c) shows that the outlines of glass fibers are well defined and distinct for the T22 composite, highlighting the good alignment of fibers in the analyzed depth. This behavior was observed for all the composites.

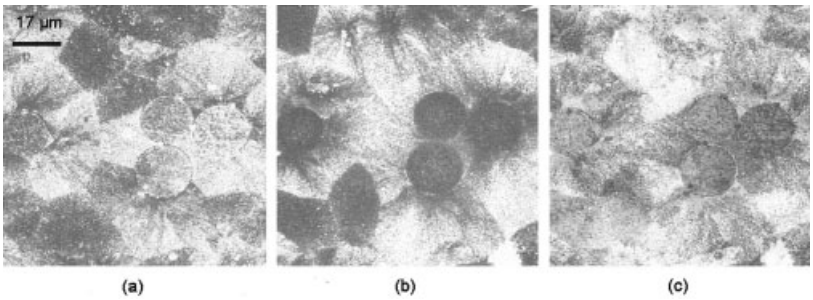

Figure 3 Confocal microscopy observations of the T22 composite: (a) at the sample surface, (b) at 100 μm of depth, and (c) the result of the difference between the images (a) and (b).

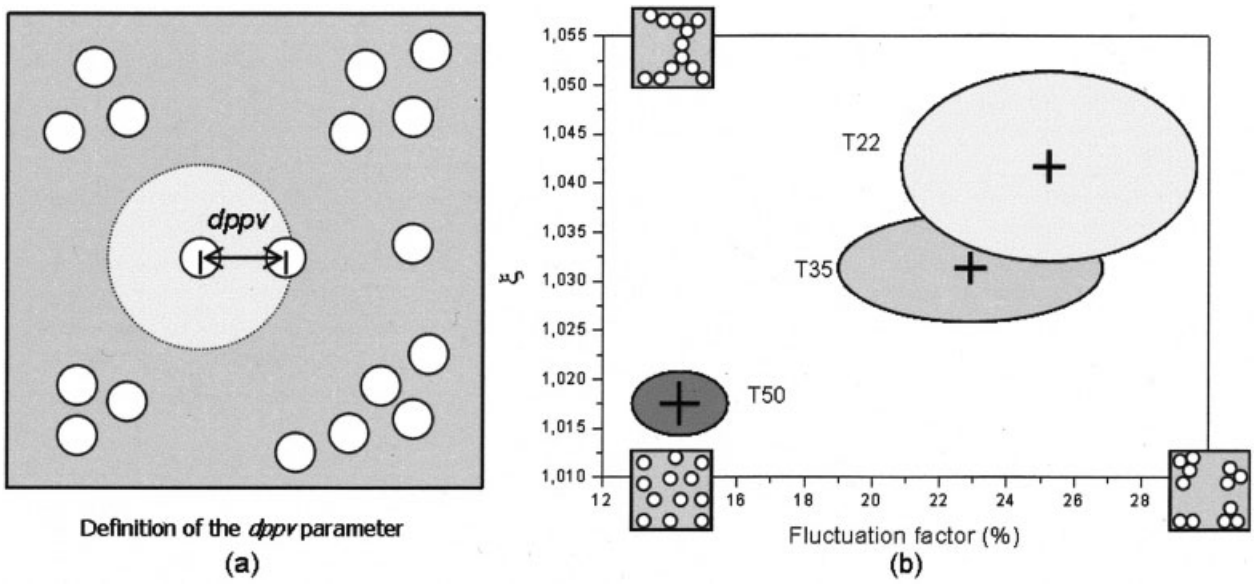

Figure 4 (a) Definition of the *dppv* parameter and (b) variation of ξ versus the fluctuation factor.

Spatial distribution of the glass fibers. Image analysis could provide accurate characterization of the 2D geometric arrangement of fibers within the polymer matrix. For example, Coster and Chermant.[27] have developed a method to determine the distance between the center of the first nearest-neighbor, the so-called *dppv*, from the coordinates of the center of gravity of each inclusion [Fig. 4(a)].

Becu[28] has defined the uniformity of the spatial distribution of core-shell particles dispersed in an epoxy resin through the determination of the two following morphological parameters:

1. the fluctuation factor is calculated from the ratio between the standard deviation of *dppv*, the so-called σ_{dppv}, to the average nearest-neighbor distance ($\overline{dppv}$),
2. the dispersion factor, ξ, is defined by the following expression:

$$\xi = \overline{dppv}(\overline{1/dppv}) \quad (1)$$

where ($\overline{1/dppv}$) is the reciprocal nearest-neighboring distance.

The fluctuation factor is all the greater as the dispersion quality of fillers is lower. The ξ parameter is equal to 1 for a perfect dispersion of fillers. Higher values of such a parameter reflect the presence of filler paths [Fig. 4(b)]. Albérola et al.[2] have applied this method to determine the spatial distribution of unidirectional glass fibers within an epoxy resin.

Figure 4(b) shows the evolution of the ξ parameter versus the fluctuation factor for the commingled composites. For each material, uncertainties are represented by the gray areas.

It can be seen that the T22 and T35 composites are characterized by high values of fluctuation and dispersion factors. These results suggest a weak quality of dispersion of glass fibers within the polypropylene matrix, in agreement with previous SEM observations [Figs. 2(a) and (b)]. In contrast, the T50 composite exhibits a more homogeneous spatial distribution of fibers, characterized by lower values of both fluctuation and dispersion factors. Such an unexpected result, i.e., an improvement of the quality of dispersion of fibers with the filler content, can be due to the decrease in the distance between aggregates. This will be shown in the next part of this paper.

However, the main drawback of the present approach is the dependence of the *dppv* parameter on the uniformity of the glass fiber diameter. Consequently, the interfiber surface-to-surface distance, δ, is then determined [Fig. 5(a)].

Figure 5(b) shows the distribution of the distance δ for the T22 composite. It varies from 0.27 μm (image resolution) to about 2.2 μm (so-called δ_{max}). The average value of the minimum distance, δ_m, quantified from the maximum of the fitted Lorentzian, is equal to about 0.55 $\pm$ 0.05 μm for all surface fractions of glass fiber (Table II). According to Gao and Mader,[29] this distance can be related to the development of regions rich in maleic anhydride groups at the vicinity of the filler surface, favoring the impregnation of glass bundles by the polymer. The amount of aggregates as a function of the total filler content, S_{fagre}, can be also evaluated by using the δ_{max} distance determined from previous image processing (Table II).

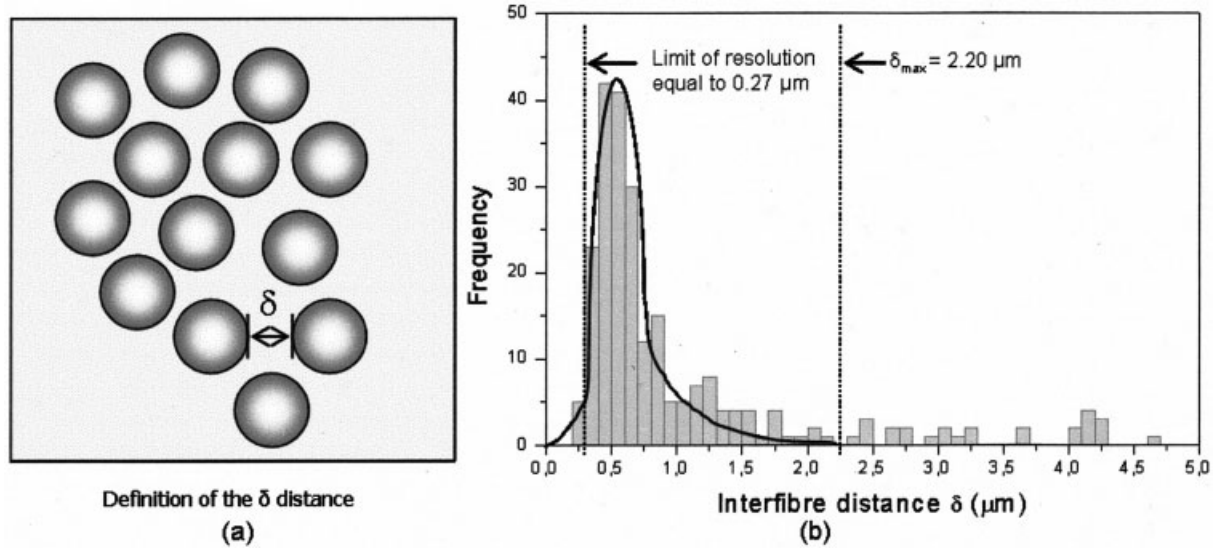

Figure 5 (a) Definition of the minimum interfiber surface-to-surface distance δ and (b) the distribution of δ for the T22 composite.

By considering that an aggregate is defined by at least three glass fibers and the interfiber surface-to-surface distance is lower than δ_{max} (between 2 and 2.5 μm), it can be observed that this ratio remains almost constant, ranging from 84 to 88% of the total filler content, for the different composites analyzed.

From the analysis of the previous morphological parameters, we can conclude that the different composites exhibit heterogeneous morphologies, characterized by the presence of fiber aggregates. The high amount of aggregates within PP matrix is promoted by

1. the nonpolar nature of the polymer,[30,31]
2. the formation of regions rich in maleic anhydride groups close to the filler surface,[29] and
3. the processing conditions.[6,7,9,10]

Now, it is interesting to define the characteristics of the aggregates, and more particularly an eventual periodic arrangement of fibers within aggregates.

To this aim, the "included angles" method has been carried out, according to the approach proposed by Yurgartis [18] [Fig. 6(a)]. This parameter is determined by taking into account the previous δ_{max} parameter.

As an example, three thin maximums in the distribution of the included angles, located at 60, 120, and 180° for the T35 composite, is depicted in Figure 6(b). This suggests that fibers are arranged according to a hexagonal motif, as described in Figure 7. Such an arrangement has also been found for the different composites analyzed and does not depend on the filler content.

The same method has been applied to reveal an eventual arrangement between aggregates in the different composites. In contrast to the previous observations, no preferential included angles have been detected whatever the fiber content. Accordingly, in the next parts of this paper, it will be assumed that aggregates are randomly dispersed within the polymer matrix.

Based on both the determination of the maximum distance between the outlines of glass fibers (δ_{max}) and the 2D arrangement of fibers into a triangular pattern, the maximum packing fraction of glass fibers in the aggregates, $S_{fmax,}$ can be determined through the following expression:

$$S_{fmax} = S_{ftheo}\left(\frac{d}{d + \delta_m}\right)^2 \quad (2)$$

where S_{ftheo} is the maximum packing of fibers in 2D and d is the average diameter of glass fibers $\approx$ 17.5 $\pm$ 0.5 μm.[3]

Previous analyses have shown that

1. the average distance, δ_m, is equal to about 0.55 $\pm$ 0.05 μm,

TABLE II
Mean δ_m and Maximum δ_{max} Interfiber Surface-to-Surface Distances[a]

Composite	δ_m (μm)	δ_{max} (μm)	S_{fagre} (%)
T22	0.54 ± 0.03	2.2 ± 0.2	84 ± 3
T35	0.55 ± 0.07	2.1 ± 0.2	88 ± 2
T50	0.60 ± 0.06	2.1 ± 0.2	85 ± 3

[a] S_{fagre} corresponds to the ratio between the amounts of aggregated fibers to the overall filler content.

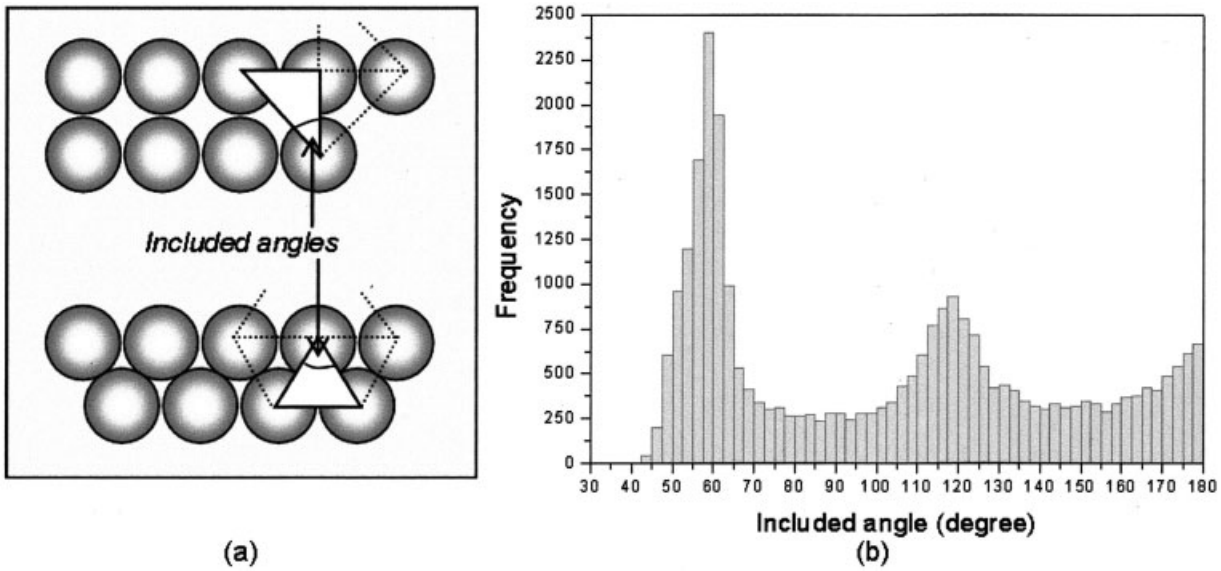

Figure 6 (a) Schematic representation of the included angles and (b) the distribution of the included angles for the T35 composite.

2. fibers are arranged according to a triangular motif, i.e., $S_{ftheo} = 0.907$ in 2D.[32]

Accordingly, the maximum packing fraction of glass fibers into aggregates is found to be about 0.84 [eq. (2)[rsqb]. This value, lower than the theoretical one, i.e., 0.907, can be related to the manufacturing conditions used for commingled composites.

Then, based on image processing analysis, we can conclude that

1. the 2D spatial distribution of the glass fibers is heterogeneous, whatever the filler content,
2. 86% of fibers are packed into aggregates,
3. the average value of the interfiber distance is equal to 0.55 μm, whatever the surface fraction of glass fiber,

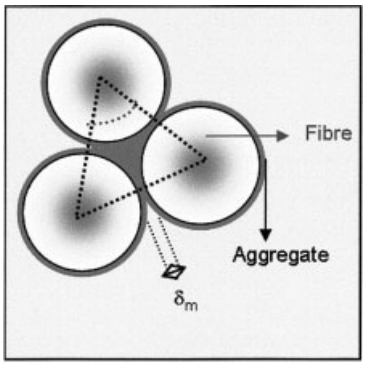

Figure 7 Scheme of the fibers arrangement in the aggregates.

4. the maximum packing fraction of glass fibers into aggregates is equal to 0.84.

At the meso scale

2D global approach. To complete this analysis, and in particular to quantify the geometric characteristics of aggregates, such as dimension and dispersion, new morphological parameters are defined. For this, a global analysis of the morphology is then proposed to determine the two following parameters:

1. the mean distance between the aggregates within the PP matrix and
2. the radii of aggregates.

These two parameters are determined from the autocorrelation function in 2D and the Fourier transform power spectra, respectively.

Thus, from the autocorrelation function, described elsewhere,[21,27] the presence of morphological periodicities in the different images can be detected. From this method able to summarize a fuzzy arrangement, the average interaggregate center-to-center distance $\bar{D}$ is evaluated (Fig. 8).

Values of this parameter $\bar{D}$ are reported in Table III for the different composites.

For the T22 and T35 composites, it can be observed that values of such a parameter, about 115 μm, are almost constant. In contrast, this distance is almost 1.5 times lower for the T50 composite, i.e., 75 μm approximately.

This result confirms that the increase in the filler content does not modify the distance between fibers,

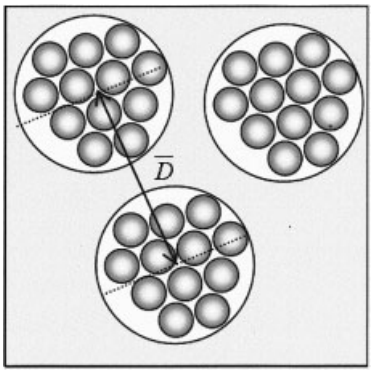

Figure 8 Definition of the interaggregate center-to-center distance $\bar{D}$.

but leads to a decrease in the distance between the aggregates. Thus, glass fibers seem to show a better dispersion in the highest filled material.

A second method, based on fast Fourier transform (FFT) technique, was used to analyze the morphology of composites at different scales. The interest of this approach is to describe the architecture of heterogeneous materials at different scales, from the size of a single fiber up to the thickness of the sample. The different steps of the processing method are depicted in Figure 9.

The FFT processing is applied to an experimental SEM image in real space [Fig. 9(a)] to give a new image encoded in the reciprocal space. This last one shows a series of rings corresponding to characteristic spatial frequencies [Fig. 9(b)]. The radial intensity distribution (RID) is then determined with the help of an accumulator recording in all the directions from the origin of the FFT image the difference of the amplitude (or the intensity) of the signal [Fig. 9(c)]. The obtained curve represents the evolution of the power or the intensity versus the spatial frequencies.

TABLE III
Mean Interaggregate Distance $\bar{D}$ for the Studied Composites

Composite	Distance $\bar{D}$ (μm)
T22	125 ± 25
T35	110 ± 25
T50	75 ± 20

To verify the accuracy of this method, the RID profile of simulated images with fibers of 17.5 μm diameter, arranged according to a crystalline motif, and called a "virtual composite," has first been analyzed (Fig. 10). The evolution of the RID profiles of the composites analyzed then were recorded.

Two regions can be distinguished:

For the high spatial frequencies beyond 0.06 μm^{-1}, corresponding to a dimension smaller than 17 μm, a good agreement between the virtual composite and experimental curves can be observed. In particular, virtual composite and analyzed materials both display a peak with an onset beginning at about 0.06 μm^{-1}. This confirms that the mean diameter of fibers is close to 17 μm and the distribution of the fiber diameters is narrow.

For the low spatial frequencies, i.e., from 0.008 to 0.06 μm^{-1}, corresponding, respectively, to 125 and 17 μm, a qualitative examination of data shows that intensity decreases with a power law, in particular for the T50 composite. By analogy with the scattering curves $I(q)$ obtained by SAXS or SANS analyses,[33] the slope of this linear region can be related to a fractal dimension of the aggregates. Values of the slopes obtained for the materials, α, are reported in Table IV.

It can be seen that the T22 and T35 composites are characterized by equivalent values of α, in contrast with the T50 composite, which exhibits a lower value. This confirms that the fiber aggregation levels displayed by the T22 and T35 composites are similar, in contrast to the T50 composite where the aggregates cannot be well distinguished because of the weak interaggregate distances.

To complete this mesoscale analysis, geometrical characteristics of the aggregates, such as their surface fraction, S_{ag}, their equivalent radii, R_{ag}, and their surface-to-surface distance, Δ_{ag}, are then evaluated. Let us recall that an aggregate is composed by at least

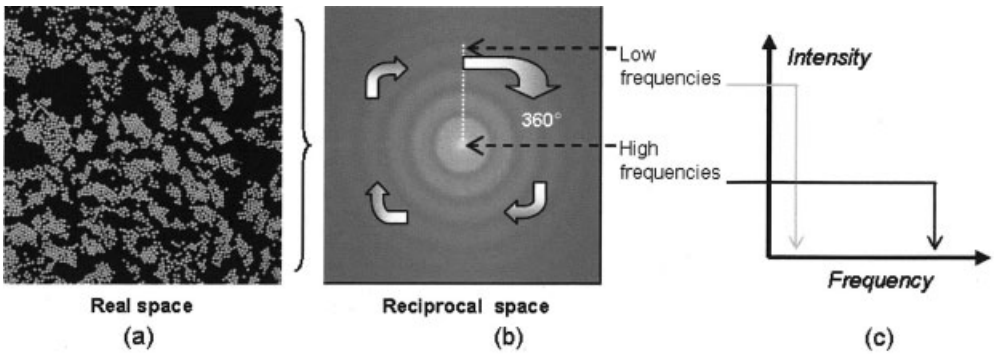

Figure 9 Processing method of the FFT approach.

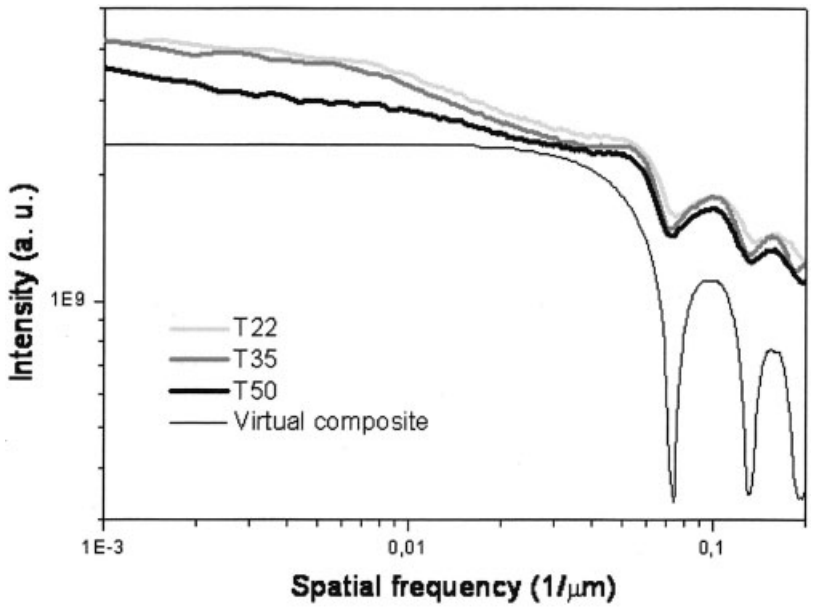

Figure 10 RID profiles of a virtual composite and of the composites analyzed.

three glass fibers and the interfiber surface-to-surface distances are lower than the δ_{max} parameter.

2D geometrical parameters of the aggregates. Based on the experimental values of the maximum interfiber surface-to-surface distance, δ_{max}, the surface fraction of fiber aggregates, S_{ag}, can be evaluated (Table V).

The determination of the radii of the aggregates, R_{ag}, requires the knowledge of both the parameter $\bar{D}$, previously determined through the autocorrelation function, and the interaggregate surface-to-surface distance Δ_{ag}. This parameter can be evaluated by using a method close to that of so-called the distance between the first nearest-neighbor, *dppv* (see Experimental quantitative morphology analysis).

Several operations of dilatation are first performed to link the different aggregates, until only one cluster appears. Then, Δ reaches a critical value defined as Δ_{ag}, which corresponds to the interaggregate surface-to-surface distance of the first nearest-neighbor. The evolution of the number of aggregates as a function of the distance required to link the different aggregates Δ are depicted on Figure 11.

With increasing filler content, it can be observed an increase in the Δ_{ag} values connected with the increase in the polymer matrix amount due to the enhancement of the interaggregate distance.

The radii of the aggregates R_{ag} can be thus evaluated through the following relationship:

$$R_{ag} = \frac{\bar{D} - \Delta_{ag}}{2} \tag{3}$$

where $\bar{D}$ is the interaggregate center-to-center distance. Experimental values of Δ_{ag} and R_{ag} are reported in Table V.

Before analyzing these data, a second method can be applied to evaluate the values of the radii of the aggregates, the so-called $R_{ag'}$. Based on the experimental values of the surface area of the different aggregates, evaluated through image processing, the radii $R_{ag'}$ can be determined by assuming that aggregates exhibit a spherical shape (Table V).

A good agreement between values of R_{ag} resulting from the two methods can be observed. This confirms the validity of the proposed approach.

In addition, as glass fiber aggregates possess a circular cross section and contact with the matrix fiber

TABLE IV
Values of the Parameter α

Composite	$\alpha(10^{-10})$
Virtual composite	0.0
T22	3.6 ± 0.4
T35	4.0 ± 0.4
T50	2.2 ± 0.4

TABLE V
Values of 2D Geometrical Parameters of Aggregates

Composite	S_{ag} (%)	Δ_{ag} (μm)	R_{ag} (μm)	$R_{ag'}$ (μm)	R_s (μm)
T22	26.0 ± 3.0	63 ± 4	31 ± 2	28 ± 3	62 ± 4
T35	42.6 ± 4.6	36 ± 4	37 ± 3	37 ± 2	55 ± 4
T50	59.9 ± 3.3	18 ± 3	30 ± 2	32 ± 3	39 ± 3

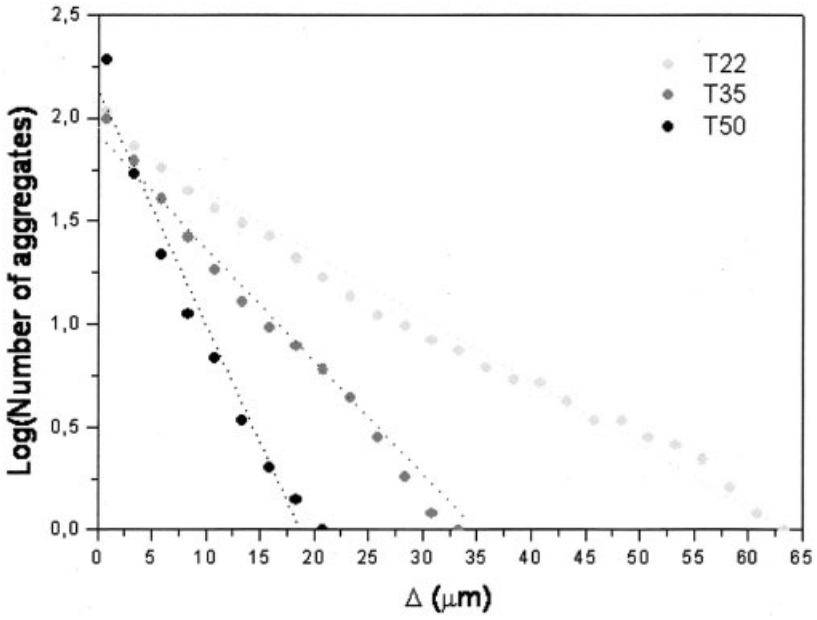

Figure 11 Determination of the interaggregate surface-to-surface distance Δ_{ag}.

bundle, the impregnation distance can be simply represented by the equivalent diameter of the glass fiber aggregate.[34] According to Bernhardsson and Shishoo,[12] the latter was found to vary from 50 to 100 μm in commingled composite materials, validating our results.

Finally, to take account of the distance between aggregates, Δ_{ag}, and the size of the aggregates, R_{ag}, the radius of the polymer shell surrounding the aggregates, R_s, can be determined according to the following relationship:

$$R_s = R_{ag} + \frac{\Delta_{ag}}{2} \tag{4}$$

In a recent work, Paar et al.[35] have also introduced the outer radius of the matrix shell, R_s, into the modeling of the mechanical behavior of unidirectionally reinforced ceramic matrix composites. Values of R_s are reported in Table V.

With increasing filler content, the radius R_s decreases, implying that the thickness of the polymer shell surrounding the fiber cluster decreases.

To confirm previous issues, it is now of interest to compare the ratio of R_{ag} and R_s determined from the processing of SEM observations and the ratio of R_{ag}^* and R_s^* evaluated from optical microscopy images for the same composites. For example, an optical microscopy image of the T22 composite is shown in Figure 12, defining the radii R_{ag}^* and R_s^*.

As shown in Table VI, a good agreement is found between the values of R_{ag}/R_s and R_{ag}^*/R_s^* derived from SEM and optical microscopy images, respectively. Moreover, with increasing the fiber amount, the R_{ag}/R_s ratio increases. This is consistent with the decrease in the interaggregate distance.

In addition, values of R_s^* evaluated through optical microscopy images can be related to the distance between the aggregate center and the limit of the spherulite growth (Fig. 12).

Then, with increasing fiber content, the proposed morphological analysis leads to the following conclusions:

1. the aggregate content S_{ag} increases,
2. the interaggregate surface-to-surface distance Δ_{ag} decreases,

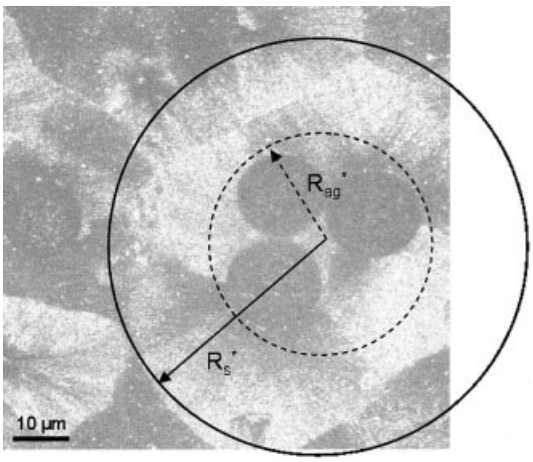

Figure 12 Optical microscopy observation of the T22 composite.

TABLE VI
Various Ratios Issue from SEM and Optical Microscopy Images

Composite	R_{ag}/R_s from SEM	R_{ag}^*/R_s^* from optical microscopy
T22	0.45 ± 0.04	0.40 ± 0.05
T35	0.67 ± 0.04	0.60 ± 0.05
T50	0.82 ± 0.03	0.85 ± 0.05

3. the radii of the aggregates R_{ag} remain almost constant,
4. the outer radii R_s decreases, due to the decrease of the thickness of the polymer shell surrounding the aggregates,
5. the R_{ag}/R_s ratio increases.

From these different morphological parameters, a scheme of the multiscale morphology of commingled composites can be proposed (Fig. 13): two levels of reinforcing phase can be considered, i.e., (i) the glass fibers at a local scale and (ii) the fiber aggregates at the mesoscale.

Prediction of the morphology evolution as a function of filler content

From previous quantitative image analysis, the morphology of composites can be described as follows: composites are reinforced by aggregates randomly dispersed within the polymer matrix. Each aggregate is constituted by fibers arranged at a maximum packing fraction (S_{fmax}) of 0.84. Fibers are surrounded by a shell of polymer. The corresponding surface fraction of polymer surrounding the aggregates is then equal to about 0.16.

Thus, at the aggregate level in 2D, a morphological parameter, χ_0, can be defined as follows:[2]

$$\chi_0 = \frac{S_{mag}}{S_f} = \frac{S_{ag} - S_{-f}}{S_f} \quad (5)$$

TABLE VII
Values of S_f, S_{ag}, S_{mag}, and χ_0

Composite	S_f	S_{ag}	S_{mag}	χ_0
T22	0.22 ± 0.02	0.26 ± 0.03	0.04 ± 0.02	0.18 ± 0.02
T35	0.35 ± 0.03	0.42 ± 0.05	0.07 ± 0.03	0.20 ± 0.03
T50	0.50 ± 0.03	0.60 ± 0.04	0.10 ± 0.03	0.20 ± 0.03

where S_{mag} is related to the polymer content into aggregates and S_f corresponds to the amount of fibers.

Data related to these parameters are listed in Table VII. As the maximum packing fraction of fibers in aggregates is about 0.84, the χ_0 value for each aggregate might be constant at about 0.19. This value is experimentally confirmed for the different commingled composites (Table VII).

As experimentally shown, with increasing fiber content, the amount of aggregates increases whereas the interaggregate distance decreases. Thus, this morphological evolution can be described by using the percolation concept.[36]

- For aggregate content ranging from 0 to the percolation threshold in 2D, S_{agc}, the surface fraction of polymer not in aggregates, S_{mp}, can be expressed by the following relationship:

$$S_{mp} = S_m - S_{mag} \quad (6)$$

where S_m (= 1 − S_f) is related to the overall surface fraction of polymer and S_{mag} corresponds to the polymer content in aggregates.

By replacing S_{mag} by its expression [eq. (5)[rsqb, $S_{mag} = \chi_0 S_f$, it yields the following equation:

$$S_{mp} = S_m(1 + \chi_0) - \chi_0 \quad (7)$$

Thus, the surface fraction of fiber aggregates in 2D, S_{ag}, can be expressed as follows:

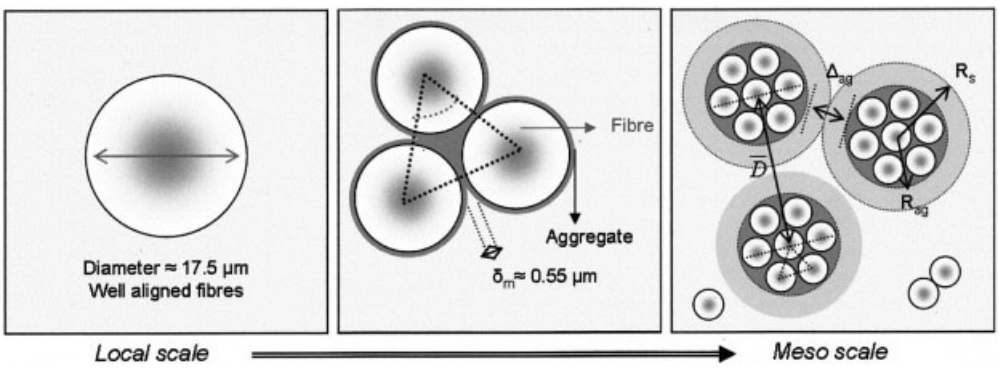

Figure 13 Scheme of the morphology of commingled composites.

$$S_{ag} = S_f + S_{mag} = S_f(1 + \chi_0) \quad (8)$$

- At the critical surface fraction of aggregates in 2D, S_{agc}, the corresponding critical polymer content, S_{mpc}, is defined by

$$S_{mpc} = S_{mc}(1 + \chi_0) - \chi_0 \quad (9)$$

where S_{mpc} is the critical amount of polymer not in aggregates and S_{mc} is the critical overall content of polymer.

By considering the fibers to be disks in 2D, it is well known that the site percolation threshold of such entities is about 0.65 in the hexagonal lattice.[32] This critical value, S_{fc}, can be related to a particular amount of fiber aggregates, S_{agc}, defined by

$$S_{agc} = S_{fc}(1 + \chi_0) \quad (10)$$

- For surface fractions of aggregates, S_{ag}, ranging from the percolation threshold, S_{agc}, to the maximum packing fraction of aggregates, S_{agmax}, the surface fraction of polymer outside the aggregates obeys the following percolation law:[36]

$$S_{mp} = S_m\left(\frac{S_m - \zeta}{\phi}\right)^{\beta} \quad (11)$$

where the critical exponent β is 0.14 in a 2D lattice.[36,37]

The constants ζ and φ are determined by the following boundary conditions:

1. At the maximum packing fraction of aggregates, all aggregates have merged and the morphology of the composite sums up to a unique cluster showing the same characteristics as the smallest aggregates, i.e., the same χ_0 value. Accordingly, $S_{ag} = S_{agmax}$ is equal to 1, leading to $S_{mp} = 0$ for $S_m = S_{mag}$, and then the ζ constant is equal to 0.16.
2. At the percolation threshold of aggregates and then for $S_{ag} = S_{agc}$, the amount of polymer outside the aggregates obeys both eq. (9) and the percolation law [eq. (11)]. Thus, the surface fraction of polymer not in aggregates in 2D can be expressed by the following relationship:

$$S_{mp} = \frac{S_m}{S_{mc}}\left(\frac{S_m - S_{mag}}{S_{mc} - S_{mag}}\right)^{\beta}(S_{mc}(1 + \chi_0) - \chi_0) \quad (12)$$

and the evolution of the amount of fiber aggregates in 2D, S_{ag}, is defined by the expression

$$S_{ag} = 1 - \left[\left(\frac{1 - S_f}{1 - S_{fc}}\right)\left(\frac{1 - S_f - S_{mag}}{1 - S_{fc} - S_{mag}}\right)^{\beta}\right][(1 - S_{fc})(1 + \chi_0) - \chi_0] \quad (13)$$

where

$$\text{where } S_{fc} = 1 - S_{mc} = \frac{S_{agc}}{1 + \chi_0} \quad (14)$$

As filler aggregate paths have not been detected within the polymer matrix even for the highest filled material, it can be concluded that the percolation threshold of aggregates, S_{agc}, has not been reached. In addition, the maximum packing content of glass fibers in commingled composites based on polypropylene was found to be about 0.84. It is well known that, for $S_{ag} > S_{agc}$, porosity drastically increases leading to the delaminating of the composite materials.[4]

Figure 14 shows the theoretical evolution of S_{ag} versus S_f processed for the following values of the morphological parameters: $\chi_0 = 0.19$, experimental values of S_f coming from SEM image analysis and $S_{mag} = 0.16$. Experimental data issue from morphology analysis are also shown for comparison.

A good agreement between experimental and theoretical evolutions of S_{ag} is found. The slope of the straight line for S_{ag} values ranging from 0 to S_{agc}, the percolation threshold of aggregates, is equal to $1 + \chi_0$. Such data confirm the self consistency of our approach.

The χ_0 value, equal to about 0.19, is insensitive to the filler content, showing the homothetic structure, i.e., aggregates dispersed within the polymer matrix. In contrast, this parameter seems to depend on both the nature of the polymer matrix and the kind of coating agent. Albérola et al.[2] have obtained higher χ_0 values (equal to about 1.00) in epoxy reinforced by raw unidirectional glass fibers. These different values can be due to the different processing conditions used for the samples analyzed. Thus, the χ_0 parameter can be considered as a probe of the manufacturing process of unidirectional composites, because it reflects the ability of polymer chains to impregnate original fiber bundles.

CONCLUSION

Based on a detailed quantitative image analysis of the 2D spatial distribution of unidirectional glass fibers within a polypropylene matrix, it has been shown that the various composites exhibit a heterogeneous morphology through different scale investigations. The morphology of these composites is then characterized by both isolated fibers and aggregates.

Thus, through the determination of accurate morphology parameters, experimental quantitative 2D im-

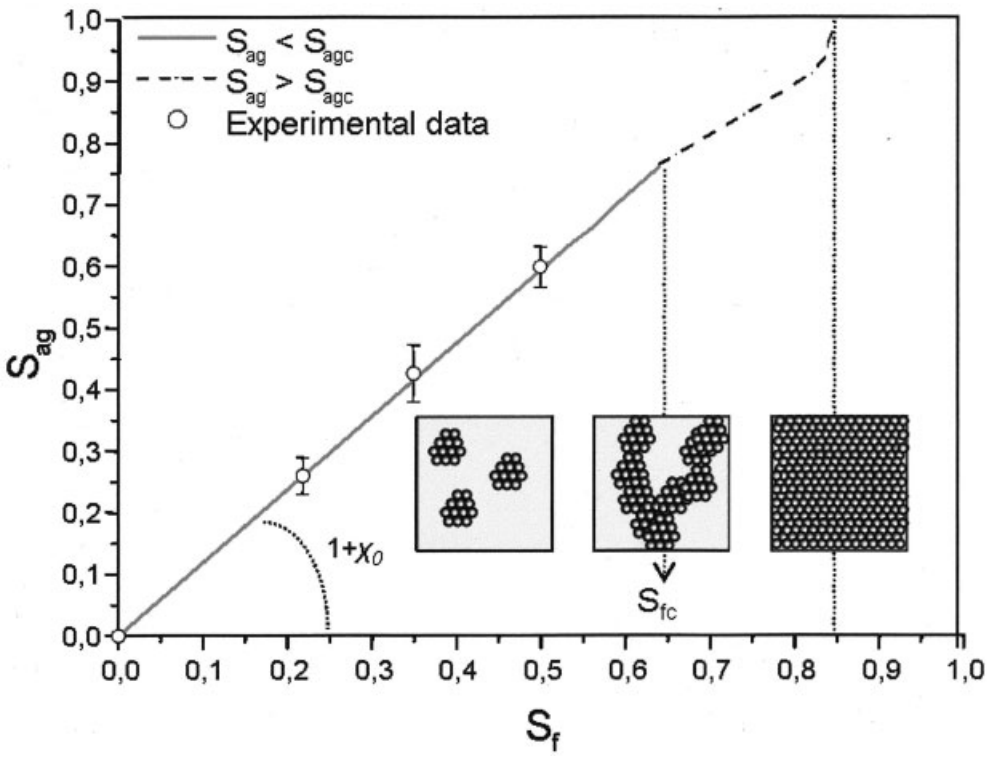

Figure 14 Experimental (○) and theoretical (- - -/—) variations of S_{ag} versus S_f.

age analysis, carried out at a local scale, revealed the following features:

1. more than 86% of fibers are packed into aggregates randomly dispersed within the polymer matrix, and
2. within aggregates, fibers exhibit a hexagonal motif and the maximum packing fraction of fibers is determined to be 0.84 for all filler contents.

A global scale morphology analysis of composites is then performed by using original methods based on the determination of the autocorrelation function and the Fourier transform power spectra.

From such analysis, the following aggregate characteristics are derived. With increasing the amount of fibers:

1. the aggregate content increases, meanwhile the distance between clusters decreases,
2. subsequently, the polymer shell surrounding the aggregates is reduced.

Based on such experimental quantitative 2D image analysis, a theoretical approach is proposed to describe the morphological evolution of composites with increasing the filler content. This is supported by the percolation concept and taking into account the presence of fiber aggregates. A good agreement is found between experimental data and theoretical issues.

In future work, we will analyze the consequences of the presence of glass fibers aggregates on the macroscopic mechanical behavior of commingled composites.

We acknowledge the assistance of M. Romeyer in taking the SEM images (LCME–University of Savoie). The contribution of M. Bernango (Centre of Quantimetry of Lyon) for help with the confocal microscopy was greatly appreciated. Finally, a special thank to M. Bollondi for helpful discussions on mathematical morphology in the elaboration of this paper.

NOMENCLATURE

W_f = weight fraction of glass fibers
V_f = volume fraction of glass fibers
S_i = surface fraction of the different phases, the indices *f*, *m*, and *p* correspond to the filler, matrix, and porosity, respectively
χ_0 = morphological parameter
dppv = distance between the nearest-neighbors of fibers
σ_{dppv} = standard deviation of *dppv*
$\overline{dppv}$ = average nearest-neighbor distance of fibers
ξ = dispersion factor

δ = minimum distance between the outlines of glass fibers
δ_m = average value of δ
δ_{max} = maximum value of δ
d = average diameter of glass fibers
$\bar{D}$ = average interaggregate center-to-center distance
α = morphological parameter
Δ_{ag} = interaggregate surface-to-surface distance
R_i = different radii of aggregates, the indices ag and s correspond to the inner and the outer radius of aggregates, respectively

References

1. Berthelot, J. M. Matériaux composites: Comportement mécanique et analyse des structures; Masson Ed.: Paris, 1992.
2. Albérola, N. D.; Merle, G.; Benzarti, K. Polymer 1999, 40, 315.
3. Dubouloz-Monnet, F.; Mélé, P.; Albérola, N. D. to appear.
4. Vendramini, J.; Mélé, P.; Merle, G.; Albérola, N. D. J Appl Polym Sci 2000, 77, 2513.
5. Long, A. C.; Wilks, C. E.; Rudd, C. D. Compos Sci Technol 2001, 61, 1591.
6. St. John, C. Proceedings of Tenth International Conference on Composite Materials; Canada, 1995; pp. 757–764.
7. Klinkmüller, V.; Um, M.-K.; Friedrich, K.; Kim, B.-S. Proceedings of Tenth International Conference on Composite Materials; Canada, 1995; pp. 397–403.
8. Mélé, P.; Vendramini, J.; Merle, G.; Albérola, N. D. ARAMM; Le Bourget du Lac: France, 1999.
9. Pagé, D. J. Y. S.; Bates, P. J.; Bui, V. T.; Bonin, H. W. J Reinforced Plastics Compos 2000, 19, 1227.
10. Wakeman, M. D.; Cain, T. A.; Rudd, C. D.; Brooks, R.; Long, A. C. Compos Sci Technol 1998, 58, 1879.
11. Bernet, N.; Michaud, V.; Bourban, P.-E.; Manson, J.-A. E. J Compos Mater 1999, 33, 751.
12. Bernhardsson, J.; Shishoo, R. J Thermoplastic Compos Mater 2000, 13, 292.
13. Bourban, P.-E.; Bernet, N.; Zanetto, J.-E.; Manson, J.-A. E. Composites: Part A 2001, 32, 1045.
14. Hou, M.; Ye, L.; Mai, Y.-W. J Mater Processing Technol 1997, 63, 334.
15. Lutz, A.; Harmia, T. Impregnation techniques for fibre bundles or tows, in Polypropylene: An A-Z Reference; Karger-Kocsis, J., Ed.; Dordrecht: Kluwer, 1999.
16. Clarke, A. R.; Archenhold, G.; Davidson, N. C. Compos Sci Technol 1995, 55, 75.
17. Paluch, B. J Compos Mater 1996, 30, 4954.
18. Yurgartis, S. W. Compos Sci Technol 1995, 52, 149.
19. Yang, S.; Tewari, A.; Gokhale, A. M. Acta Metall 1997, 45, 3059.
20. Yang, S.; Gokhale, A. M.; Shan, Z. Acta Metall 2000, 48, 2307.
21. Dubouloz-Monnet, F.; Grillet, A. C.; Lambert, P.; Merle, G., Polymer Testing, submitted.
22. Benzarti, K. Sci. thesis, Université Claude Bernard, Lyon 1997; 239 pp.
23. Van West, B. P.; Byron Pipes, R.; Advani, S. G. Polym Compos 1991, 12, 417.
24. Dubouloz-Monnet, F.; Bas, C.; Albérola, N. D. J Macromol Sci, Phys 2002, B41, 671.
25. ImageJ, http://rsb.info.nih.gov/ij/.
26. Scion Image, http://www.scioncorp.com.
27. Coster, M.; Chermant, J. L. Précis d'analyse d'images; Presses du CNRS: Paris, 1989.
28. Becu, L. Sci. thesis, Institut National des Sciences Appliquées, Lyon, 1996; 262 pp.
29. Gao, S.-L.; Mader, E. Composites: Part A 2002, 33, 559.
30. Roux, C.; Denault, J.; Champagne, M. F. J Appl Polym Sci 2000, 78 2047.
31. Van Den Oever, M.; Peijs, T. Composites: Part A 1998, 29A, 227.
32. Torquato, S. J Mech Phys Solids 1998, 46, 1411.
33. Beaucage, G.; Ulibarri, T. A.; Black, E. P.; Schaefer, D. W. In Hybrid Organic–Inorganic Composites; American Chemical Society: Washington, D.C., 1996; p. 97.
34. Sakaguchi, M.; Nakai, A.; Hamada, H.; Takeda, N. Compos Sci Technol 2000, 60, 717.
35. Paar, R.; Vallés, J.-L.; Danzer, R. Mater Sci Eng 1998, A250, 209.
36. De Gennes, P. G. Scaling Concepts in Polymer Physics; Cornell University Press: Ithaca, NY, 1979.
37. Stauffer, D. Introduction to Percolation Theory; Institute of Theoretical Physics, Cologne University; Taylor & Francis: London, 1985.